This is a repository copy of *Strangeness Photoproduction on Quasifree Neutrons : Proceedings of the 10th International Workshop on the Physics of Excited Nucleons (NSTAR2015)*.

White Rose Research Online URL for this paper:
https://eprints.whiterose.ac.uk/135902/

Version: Accepted Version

Article:

Werthmüller, Dominik orcid.org/0000-0001-6406-284X (2016) Strangeness Photoproduction on Quasifree Neutrons : Proceedings of the 10th International Workshop on the Physics of Excited Nucleons (NSTAR2015). JPS Conference Proceedings.

https://doi.org/10.7566/JPSCP.10.032008

Strangeness Photoproduction on Quasifree Neutrons

Dominik Werthmüller[1] on behalf of the A2 Collaboration

[1]*School of Physics and Astronomy, University of Glasgow, Glasgow G12 8QQ, United Kingdom*

E-mail: dominik.werthmueller@glasgow.ac.uk

Strangeness photoproduction in the elementary reactions $\gamma N \to KY$ offers the possibility to study nucleon resonances in the mass region above 1.7 GeV, where the number of states and their properties are still under debate. These reactions could allow the first "complete" experiment in pseudoscalar meson photoproduction due to the easier access to recoil polarization observables in experiments. In addition to measurements on proton targets, a full isospin decomposition of the $I = 1/2$ electromagnetic amplitudes requires also data obtained from quasifree neutron targets. This contribution shows first preliminary results on feasibility studies for such measurements at the A2 experiment at MAMI.

KEYWORDS: strangeness, photoproduction, quasifree, neutron

1. Introduction

Current experimental activities in light baryon spectroscopy at experiments such as A2 (MAMI), CB and BGO-OD (ELSA), CLAS (JLab), and LEPS (SPring-8) concentrate on the extraction of polarization observables for meson photoproduction reactions using polarized beams and/or polarized targets. In principle, a minimum set of eight carefully chosen observables would allow the determination of an unambiguous solution in terms of the involved amplitudes for pseudoscalar meson production ("complete" experiment) [1]. Because of finite uncertainties of the experimental data, it is favorable to have information about as many observables as possible to remove ambiguities. Regarding beam and target polarization observables, a large number of results are expected to be published for nonstrange meson photoproduction in the coming years. The measurement of recoil polarization observables for these reactions is more challenging since it requires a dedicated polarimeter in the experimental setup. On the other hand a "complete" measurement cannot just be any eight observables but it is necessary that at least one observable is from beam-recoil or target-recoil experiments. These can be extracted more easily in strangeness photoproduction reactions $\gamma N \to KY$ because of the self-analyzing weak decay of the hyperons Y. Therefore, the "complete" experiment could be achieved earlier with respect to the nonstrange sector. Nevertheless, measurements involving strangeness suffer from lower cross sections and additional complications related to the detection of kaons and hyperons. Consequently, the experimental database lacks of precision and coverage in terms of photon energy and kaon center-of-mass polar angles. This is especially true at threshold, where the theoretical interpretation is more straightforward, and the situation should be improved in this regard.

Due to the electromagnetic formation in photoproduction, a reliable isospin decomposition of the amplitudes is only possible when experimental data for all six possible reactions are available:

$$(1)\ \gamma p \to K^+\Lambda \quad (2)\ \gamma p \to K^+\Sigma^0 \quad (3)\ \gamma p \to K^0\Sigma^+$$
$$(4)\ \gamma n \to K^0\Lambda \quad (5)\ \gamma n \to K^0\Sigma^0 \quad (6)\ \gamma n \to K^+\Sigma^-$$

Particularly for the reactions (4)–(6) on the neutron, the experimental database is still sparse [2–6]. Concerning the study of resonance contributions in the s-channel, reactions (4) and (5) are of special interest because there are no K^0 background terms in the t-channel. Therefore, even if resonance con-

tributions are small close to threshold, a good knowledge of those reactions could help to constrain $u-$ and $t-$channel background terms in the theoretical models [7, 8]. In addition, experimental data very close above the reaction threshold provide a precision test of Chiral Perturbation Theory including the strangeness degree of freedom [9, 10]. Finally, measurements of strangeness photoproduction on bound nucleons may offer the possibility to study the KN and YN potentials via final state interaction (FSI) [11]. A good understanding of the latter is crucial for the study of hypernuclei for example.

For this contribution, existing experimental data from the A2 experiment at MAMI was analyzed to investigate the feasibility of precision measurements of strangeness photoproduction focussing on $\gamma n \rightarrow KY$ using deuterium as quasifree neutron target.

2. Experimental Setup

The A2 experiment is located at the MAMI continuous-wave electron accelerator facility in Mainz (Germany) [12, 13]. A high intensity photon beam is created from the 1.5 GeV primary beam by the bremsstrahlung tagging technique using the Glasgow photon tagger [14–16]. After beam collimation the photons impinge on the liquid deuterium target installed in the center of the sphere-like electromagnetic calorimeter Crystal Ball (CB) [17]. This detector consists of 672 NaI(Tl) crystals and provides basic tracking via a multi-wire proportional chamber (MWPC) and charged particle discrimination via a dE/E analysis using a cylinder of plastic scintillator strips (PID [18]) surrounding the target. The forward hole of CB is covered by the hexagon-shaped TAPS detector wall [19, 20]. It comprises 366 BaF_2 and 72 $PbWO_4$ crystals. Charged particles can be vetoed by plastic scintillator tiles installed in front of the crystals. Particle identification can be achieved via dE/E, time-of-flight, and pulse-shape (slow/fast scintillation light component in BaF_2) analyses. The experimental trigger used to obtain the data for this work consisted of an energy sum condition ($E_{tot} > 300$ MeV in CB) and a condition (> 2) on the activated logical sectors (45 sectors in CB, 6 sectors in TAPS).

3. Analysis

3.1 Event Selection

An overview of the event selection for the three analyzed $\gamma n \rightarrow KY$ reactions can be found in table I. The neutral K^0 was identified via the $K_S^0 \rightarrow \pi^0\pi^0$ decay ($\Gamma_i/\Gamma = 30.69\%$ [21]). Therefore, four photons from the K_S^0 decay were requested for reactions (4) and (5). An additional photon was requested in the selection for reaction (5) coming from the radiative decay $\Sigma^0 \rightarrow \gamma\Lambda$ of the Σ^0 hyperon ($\Gamma_i/\Gamma \approx 100\%$ [21]). The Λ hyperon present in both reactions was detected via demanding a proton and a pion originating from the $\Lambda \rightarrow p\pi^-$ decay ($\Gamma_i/\Gamma = 63.9\%$ [21]). Charged and neutral particles were discriminated via the PID and veto detectors. Proton and pion candidates were identified via a dE/E analysis (no charge separation possible for pions).

Event candidates for reaction (6) were filtered via the presence of an in-crystal muonic decay of a K^+ meson (see next subsection) plus a coincident neutral cluster (neutron candidate), and a charged pion cluster identified via a dE/E analysis (π^- candidate).

Table I. Overview of the event selection for the analyzed $\gamma n \rightarrow KY$ reactions.

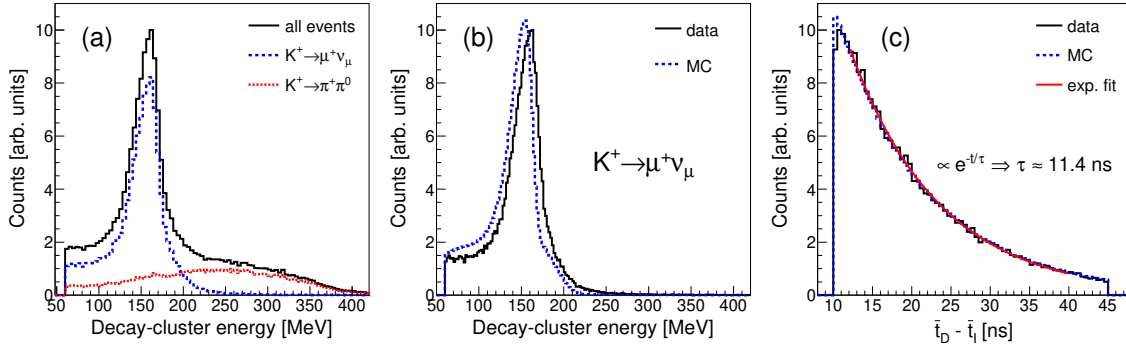| Reaction	Particle Decays	Detected Particles
(4) $\gamma n \rightarrow K^0\Lambda$	$K_S^0 \rightarrow \pi^0\pi^0$, $\Lambda \rightarrow p\pi^-$	$4\gamma p\pi^-$
(5) $\gamma n \rightarrow K^0\Sigma^0$	$K_S^0 \rightarrow \pi^0\pi^0$, $\Sigma^0 \rightarrow \gamma\Lambda$	$5\gamma p\pi^-$
(6) $\gamma n \rightarrow K^+\Sigma^-$	$K^+ \rightarrow \mu^+\nu_\mu$ (in crystal), $\Sigma^- \rightarrow n\pi^-$	$K^+n\pi^-$

Fig. 1. K^+ detection in the Crystal Ball: (a) Energy distribution of the K^+ decay clusters of all events (black solid), pionic decay events (blue dotted) and muonic decay events (red dashed). (b) Comparison of experimental (black solid) and simulated (blue dotted) decay cluster energy distributions for muonic decay events. (c) Impact-decay cluster time difference: Experimental (black solid) and simulated (blue dotted) distributions. Exponential fit to experimental data (red curve).

3.2 K^+ Detection via In-Crystal Decay

K^+ mesons were detected using their decay inside the NaI(Tl) crystal of CB after a mean lifetime of 12.38 ns [21] using the technique described in [22]. This technique splits potential K^+ clusters into impact and decay subclusters based on the timing signals. Energy and direction of the kaon can then be accessed via the impact cluster, while properties of the decay cluster help to differentiate between the dominant $\mu^+\nu_\mu$ ($\Gamma_i/\Gamma = 63.55\%$) and $\pi^+\pi^0$ ($\Gamma_i/\Gamma = 20.66\%$) [21] decays.

Fig. 1 shows some characteristic distributions related to the K^+ detection technique. In (a), the decompositon of the total decay cluster energy distribution (black histogram) into the contributions of the muonic (blue histogram) and the pionic (red histogram) decays is illustrated. A clear peak around 150 MeV due to the energy deposited by the μ^+ can be seen, whereas the distribution coming from the pionic decay is broader. Fig. 1(b) shows the good agreement of the experimental and the simulated distributions in case of the muonic decay. Only an overall energy loss correction seems to be necessary to account for the systematic shift. Finally, the time difference between the impact and the decay cluster is plotted in Fig. 1(c) for experimental and simulated data. As expected, both distributions follow an exponential drop-off and the decay time extracted from the experimental data is in good agreement with the mean lifetime of the K^+ meson.

3.3 Particle Reconstruction and Analysis Cuts

The Λ hyperon was reconstructed from the detected proton and π^- candidates. Since the energy calibration of the calorimeters was optimized for photons, and the relation between kinetic energy and deposited energy is nonlinear for low energetic hadrons, an energy correction needs to be determined and applied. In addition, a cut-off in terms of deposited energy has to be added to remove punch-through particles, which deposit less than their kinetic energy. For π^- mesons, an additional cut rejecting clusters consisting of more than four crystals was applied to improve the energy resolution by removing energy depositions from secondary reactions [23].

A clear peak around the nominal Λ mass of about 1116 MeV can be seen in the $p\pi^-$ invariant mass of Fig. 2(a). The agreement between the experimental and simulated distribution seems to be quite good for the more selective $K^0\Sigma^0$ event candidates, whereas some more background is remaining in the $K^0\Lambda$ events. All complementary analysis cuts were applied to obtain the presented distributions. A cut around the Λ peak (vertical lines) was used to select good event candidates.

The neutral kaon was reconstructed from the four detected decay photon candidates using a kinematic fit testing the hypothesis $K^0 \to \pi^0\pi^0 \to 4\gamma$. All photon combinations were fitted and the one
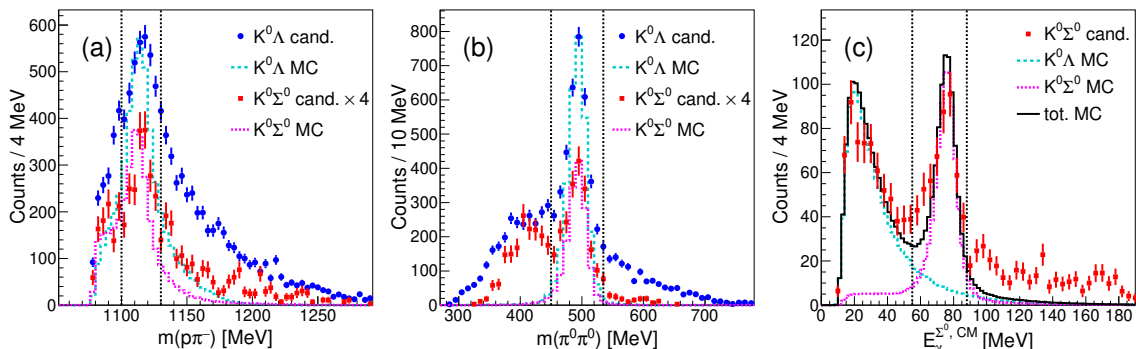
Fig. 2. Particle reconstruction distributions: Color code: blue circles (red squares): experimental distributions for $K^0\Lambda$ ($K^0\Sigma^0$) event candidates. Cyan dashed (magenta dotted) histograms: simulated distributions for $K^0\Lambda$ ($K^0\Sigma^0$) events. (a) $p\pi^-$ invariant mass showing the Λ signal. (b) $\pi^0\pi^0$ invariant mass showing the K^0 signal. (c) Energy distribution of the decay photon from $\Sigma^0 \to \gamma\Lambda$ in the rest frame of the Σ^0 hyperon.

with the smallest χ^2 was selected as good K^0 candidate. As can be seen in Fig. 2(b), a clear peak coming from the K^0 is visible in the $\pi^0\pi^0$ invariant mass distributions. The composition of the remaining background events still needs to be studied. All complementary analysis cuts were applied to obtain the presented distributions. A cut around the K^0 peak (vertical lines) and additionally a cut in the 2γ invariant masses selecting two good π^0 candidates (not shown here) were introduced in the analysis.

The additional photon detected for the $K^0\Sigma^0$ event candidates was checked to originate from the $\Sigma^0 \to \gamma\Lambda$ decay by calculating its energy in the rest frame of the Σ^0 candidate. The resulting distribution shown in Fig. 2(c) reveals a clear peak around 76 MeV consistent with the Σ^0-Λ mass difference, and agrees with the distribution obtained from simulation. The background contribution at low energies is nicely described by the $K^0\Lambda$ simulation where probably artificial photon clusters from split-off effects are generated. All complementary analysis cuts were applied to obtain the presented distributions. A cut around the peak (vertical lines) was used to select good event candidates.

The detection of the π^- and the neutron decay products of the Σ^- hyperon are rather challenging with the detectors of the A2 experiment. Neutron detection efficiencies in CB are below 40% [24] and the neutron kinetic energy can only be measured via time-of-flight in the forward TAPS wall. Nevertheless, in case of the quasifree reaction on the neutron in $\gamma d \to K^+\Sigma^-(p)$, by measuring the neutron direction along with the directions and energies of the K^+ and the π^-, it is possible to calculate the neutron energy from kinematics [25], although the resolution is additionally smeared due to the secondary Σ^- decay vertex.

Further cuts applied in the analysis were the condition for the kaon-hyperon coplanarity (requesting a difference of 180° in the azimuthal angles in the lab frame) and the request for a missing proton in the $\gamma d \to KYX$ missing mass.

4.   Very Preliminary Results

Very preliminary results in terms of missing mass distributions for the $\gamma n \to K^0 Y$ reactions are shown in Fig. 3. The experimentally obtained distributions can for most parts be reasonably described by the sum of the simulated distributions of both reactions. Because the two event classes differ only in the detection of the additional decay photon of the Σ^0 hyperon, there is contamination of the $K^0\Lambda$ and $K^0\Sigma^0$ final states in both directions. Therefore, the most suited approach is probably a simultaneous yield extraction for both reactions from the distributions of the two event classes.

In the analysis of the $\gamma n \to K^+\Sigma^-$ reaction, the signal of the Σ^- hyperon can be searched in either the $n\pi^-$ invariant mass or the $\gamma n \to K^+X$ missing mass. Both distributions are shown in Fig. 4. The
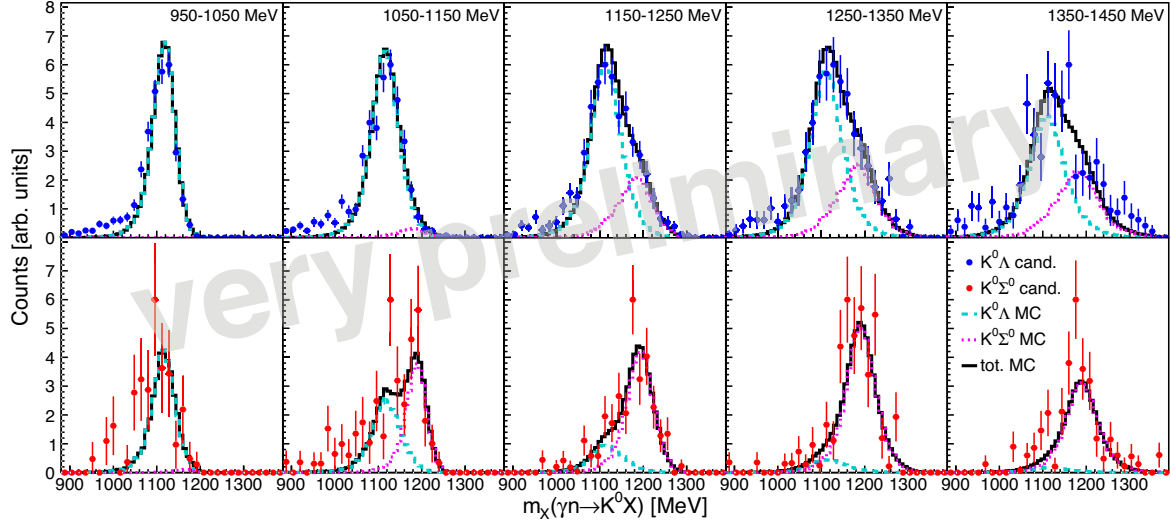
Fig. 3. Missing mass distributions of $\gamma n \to K^0 X$ for different bins of incoming photon beam energy: Color code: blue circles (red squares): experimental distributions for $K^0\Lambda$ ($K^0\Sigma^0$) event candidates. Cyan dashed (magenta dotted) histograms: simulated distributions for $K^0\Lambda$ ($K^0\Sigma^0$) events. Upper row: $K^0\Lambda$ event candidates. Lower row: $K^0\Sigma^0$ event candidates.
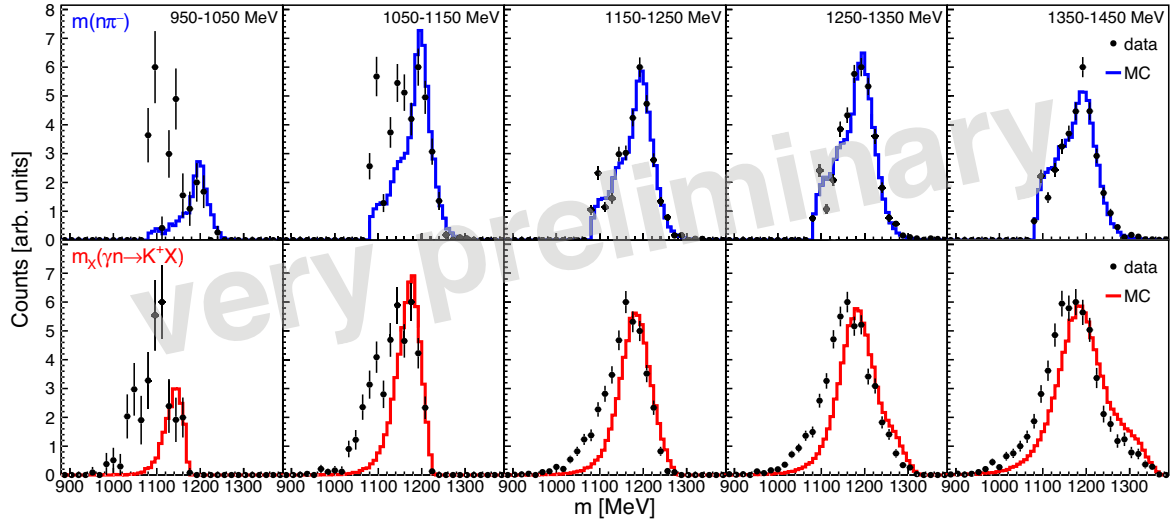

Fig. 4. Σ^- mass distributions for different bins of incoming photon beam energy: Upper row: $n\pi^-$ invariant mass experimental (black circles) and simulated (blue histograms) distributions. Lower row: $\gamma n \to K^+ X$ missing mass experimental (black circles) and simulated (red histograms) distributions.

resolution seems to be comparable for lower photo beam energies, while the resolution in the $n\pi^-$ invariant mass seems to be better for higher energies. Besides a systematic shift in the missing mass distributions due to the yet missing K^+ energy correction, the agreement between the experimental and simulated distributions is surprisingly good considering the early stage of the analysis. The remaining background in the lower photon energy bins still needs to be investigated.

5. Summary and Outlook

Very preliminary analyses of all three isospin reactions $\gamma n \rightarrow KY$ in quasifree kinematics using data from the A2 experiment obtained with a deuterium target give promising results regarding their identification. More refinements and corrections, especially concerning the detection of charged particles, should further improve the results. After optimizing the analyses in terms of statistical quality and systematic uncertainties, it remains to be seen if cross section and recoil polarization observables can be extracted from the existing data or if new measurements should be carried out.

6. Acknowledgments

References

[1] W.-T. Chiang, F. Tabakin, Phys. Rev. C **55** (1997) 2054.
[2] H. Kohri *et al.*, Phys. Rev. Lett. **97** (2006) 082003.
[3] S. Anefalos Pereira *et al.*, Phys. Lett. B **688** (2010) 289.
[4] K. Tsukada *et al.*, Phys. Rev. C **78** (2008) 014001; Phys. Rev. C **83** (2011) 039904.
[5] H. Kanda *et al.*, Nucl. Phys. A **835** (2010) 317.
[6] Futatsukawa *et al.*, EPJ Web of Conferences **20** (2012) 02005.
[7] T. Mart, Phys. Rev. C **83** (2011) 048203.
[8] T. Mart, Phys. Rev. C **90** (2014) 065202.
[9] S. Steininger, U.G. Meißner, Phys. Lett. B **391** (1997) 446.
[10] B. Borasoy *et al.*, Eur. Phys. J. A **34** (2007) 161.
[11] P. Vancraeyveld *et al.*, Nucl. Phys. A **897** (2013) 42.
[12] H. Herminghaus *et al.*, Nucl. Instrum. Methods **138** (1976) 1.
[13] K.-H. Kaiser *et al.*, Nucl. Instrum. Methods Phys. Res., Sect. A **593** (2008) 159.
[14] I. Anthony *et al.*, Nucl. Instrum. Methods Phys. Res., Sect. A **301** (1991) 230.
[15] S.J. Hall *et al.*, Nucl. Instrum. Methods Phys. Res., Sect. A **368** (1996) 698.
[16] J.C. McGeorge *et al.*, Eur. Phys. J. A **37** (2008) 129.
[17] A. Starostin *et al.*, Phys. Rev. C **64** (2001) 055205.
[18] D. Watts, Calorimetry in Particle Physics, Proceedings of the 11th International Conference, Perugia, Italy, 2004 (World Scientific, Singapore, 2005), 560.
[19] R. Novotny, IEEE Trans. Nucl. Sci. **38** (1991) 379.
[20] A.R. Gabler *et al.*, Nucl. Instrum. Methods Phys. Res., Sect. A **346** (1994) 168.
[21] K.A. Olive *et al.* (Particle Data Group), Chin. Phys. C **38** (2014) 090001.
[22] T.C. Jude *et al.*, Phys. Lett. B **735** (2014) 112.
[23] A. Marín *et al.*, Nucl. Instrum. Methods Phys. Res., Sect. A **417** (1998) 137.
[24] M. Martemianov *et al.*, JINST **10** (2015) T04001.
[25] D. Werthmüller *et al.*, Phys. Rev. C **90** (2014) 015205.